Real-time self-monitoring properties in 3D printed continuous carbon fiber reinforced thin-walled composite structures under large deformation

Abstract: Deformation monitoring is a crucial approach to ensuring safety and reliability of thin-walled structures. In this study, an electrical-resistance-based deformation monitoring method was utilized for real-time structural health monitoring of 3D printed continuous carbon fiber reinforced thin-walled composite structures. The correlation between deformation and electrical resistance changes was investigated in quasi-static lateral and axial compression for the composite structures with three different layer heights. Results showed that the mechanical–electrical behaviors during lateral and axial compression processes manifested distinct forms. A bilinear relationship between relative resistance change and compression displacement during lateral compression was obtained. Furthermore, the composite structures with lower layer heights demonstrated a higher linear correlation coefficient. Under axial compression, the relative resistance change showed a fluctuating fall/rise pattern. This pattern was associated with intricate damage morphology observed in the composite structures, such as fiber-to-fiber contact, fiber breakage, and fiber pull-out. In addition, the relative resistance change demonstrated a falling-rising pattern in the composite structures with a layer height of 0.3 mm, while it exhibited a falling-rising-falling pattern with other layer heights. The established correlation between the relative resistance change and deformation could facilitate real-time self-monitoring of deformation and failure states in thin-walled structures.

1. Introduction

Thin-walled structures were widely used in automotive, aerospace, and other industries as efficient energy absorption devices due to their excellent lightweight and energy absorption capacity [1-3]. In recent years, the growing concerns regarding fuel consumption, environmental pollution, and crash safety have significantly amplified the quest for lighter and more reliable energy-absorbing structures [4, 5]. Continuous carbon fiber reinforced composites (CFRCs) have attracted increased attention for their outstanding performance-to-weight ratio[6-8]. Consequently, many studies have been carried out to investigate the crashworthiness characteristics of CFRC-based energy-absorbing structures , which demonstrated superior energy-absorbing efficiency [7-9]. Nevertheless, beside pursuing high mechanical properties, it was also crucial to ensure the safety and reliability of the thin-walled structures [10].

In practical applications, the accumulation of plastic deformation and damage to thin-walled structures due to the collision was inevitable, which may result in catastrophic events [11]. To ensure operational safety, classical techniques such as non-destructive testing (NDT), vibration/modal based methods, and structure health monitoring (SHM) systems consisting of actuator-sensor networks were developed to monitor the states of thin-walled structures [12, 13]. Nonetheless, the use of sensors embedded in or attached to materials (extrinsic smartness) presents challenges, including increased costs, reduced durability, and compromised mechanical properties. [14, 15]. The mechanical-electrical behavior of continuous carbon fiber offers the potential for self-monitoring through electrical-based damage detection technologies,

addressing the above issues. This feature is considered crucial for enabling the integrated design of structural augmentation and real-time health monitoring in CFRC-based structures [16].

Typically, the electrical resistance of continuous carbon fiber shows a linear increase with tensile strain, a linear decrease with compressive strain, and an irreversible increase upon damage [17]. In early studies, mechanical-electrical behaviors of CFRCs were also preliminarily investigated under tension [18, 19], shear [20], and flexure [19, 21-23] conditions, which proved the feasibility of the electrical resistance detection technique on self-monitoring of material states. Furthermore, in addition to measuring resistance along fiber orientation, damage self-monitoring can be achieved by measuring the through-thickness resistance and the oblique resistance [24]. The recent advancement in 3D printing technology has not only expanded the design space but also offered innovative possibilities for the evolution and development of self-monitoring CFRCs[25, 26][27, 28]. Cheng et al. [12] introduced a novel self-monitoring approach for the detection and characterization of fiber damage during the 3D printing of CFRCs. An observable increase in the electrical resistance was primarily detected, indicating fiber damage attributed to the combination of excessive printing speeds and extrusion rates, along with insufficient layer heights and printing temperatures. Wang et al. [29] developed a smart sensing system for a continuous carbon fiber (CCF)-thermoplastic lattice truss sandwich structure to determine the strain, stress, and damage of the structure based on the electric-mechanical behavior of CCF. However, the mechanical-electrical behaviors of 3D printed continuous carbon

fiber reinforced thin-walled composite structures (CCFTCSs) in practical applications are complex and differ from the standard tests mentioned above. Consequently, it was necessary to study the mechanical-electrical relationship of CCFTCSs under loadingthat are more closely aligned with actual operating conditions.

In this study, CCFTCS samples was fabricated through 3D printing and their mechanical-electrical behaviors of were investigated to understand the relationship between the electrical resistance change and the load scenario. Kelvin Four-terminal sensing method was applied to continuously supervise the evolution of electrical resistance in the specimens with three different layer thicknesses under quasi-static lateral and axial compression tests. The multiscale morphological investigation was also employed to quantify the relationship between the electric resistance and deformations.

2. Experimental method

2.1. Materials and processing

In this study, the polylactic acid (PLA, eSUN, Shenzhen, China) filament, with a standard diameter of 1.75 mm, was utilized as the matrix material. The polyacrylonitrile (PAN)-based continuous carbon fiber (CCF, T300B-1000-50B, Toray Co., Ltd., Tokyo, Japan) was utilized as both the reinforcement and structure monitoring elements for the 3D printed CCFTCSs.

A modified commercial 3D printer (Ender3 V2, Creality 3D Technology Co., Ltd, Shenzhen, China) with a single 1.3 mm diameter flat-head nozzle was used to manufacture the CCFTCSs. **Fig.1** (a) presents schematically the principle of the fused

filament fabrication (FFF) technique, which synchronously receives PLA filament and continuous carbon fiber to manufacture the CCFTCSs. The printed CCFTCSs are cylindrical with an outer diameter (D) of 50 mm [30], and a height (H) of 20 mm. The thickness is around xxx mm resulting from the nozzle size. The printing speed was set as 100 mm/min following our previous study [31], and the print temperature was selected as 210 ℃ as suggested by the filament supplier. The layer thicknesses of the CCFTCSs were selected at 0.3 mm, 0.4 mm, and 0.5 mm [31], which are printable using our equipment and materials while enabling a thorough study on the impact of layer thickness. Following the completion of the 3D printing process, electrodes were connected to the ends of the continuous carbon fiber sensing element as shown in **Fig .1** (b), where the carbon fiber and copper wires were bonded with conductive silver paste (MECHANIC Co., Hong Kong, China) to obtain a stable electrical signal.

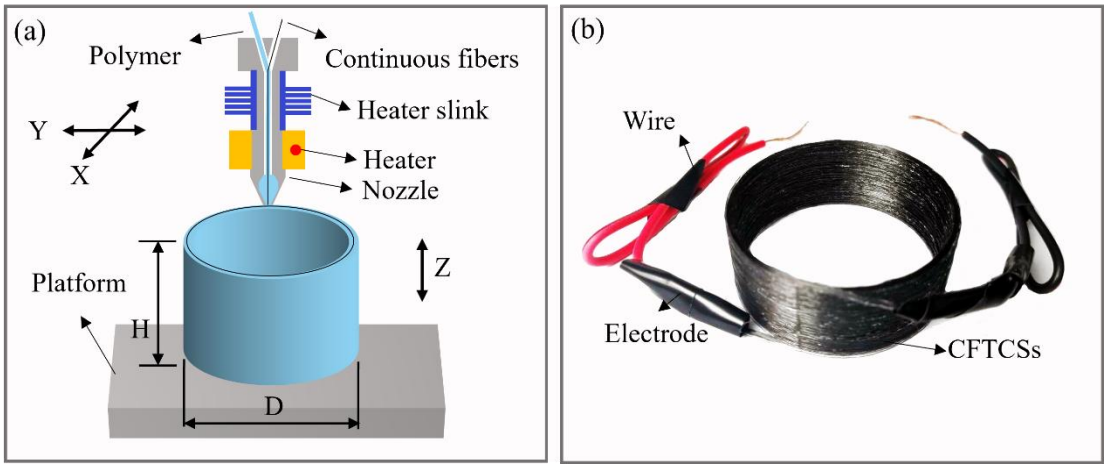

Fig. 1 (a) schematic of the 3D printing process; (b) the produced smart CCFTCSs with electrodes.

2.2. Experimental measurement

To analyze the mechanical-electrical behaviors of the CCFTCSs, quasi-static lateral and axial compression tests were performed using a universal mechanical testing machine (E44, MTS Co, USA). As shown in **Fig.** 2 (a) and (b), the specimens were compressed vertically by two rigid and flat platforms. The top platform moved down at a constant velocity of 5 mm/min during the test [32]. The final displacement for the quasi-static compression was 70% of the original length (35 mm for lateral compression and 14 mm for axial compression, respectively). The entire collapse process for all CCFTCS samples was captured on videousing a digital camera (EOS 5D, Mark IV, Canon, Japan). In addition, the damage patterns and the failure details of the CCFTCSs under compression were observed with an optical microscope (AO-3M150GS, AOSVI, Shenzhen, China).

The electrical signal of the CCFTCSs during the compression tests was measured at room temperature using the Kelvin Four-terminal sensing method, as depicted in Fig. 2(c). In this method, a constant current is supplied through the outer two probes, and the voltage induced by this current is measured using the inner two probes. This methodology significantly mitigates the impact of contact electrical resistance, thereby enhancing the precision of resistance measurements during compression testing. As shown in **Fig.2** (d), a KeySight Agilent 34970A data collector was used to measure the real-time electrical resistance of the CCFTCSs. The experiment commenced 30 minutes after energizing the test bench to mitigate potential temperature-induced zero drift effects on carbon fiber resistance, which could impact the experimental outcomes [33].

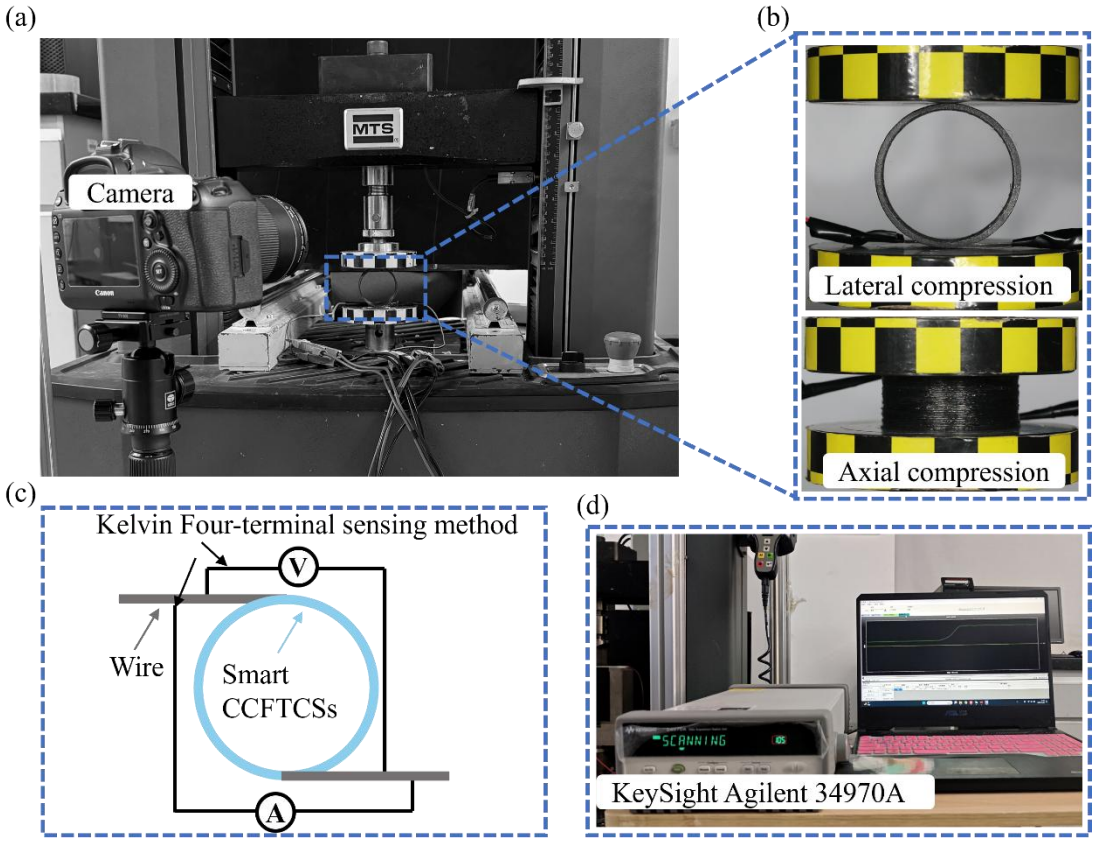

Fig. 2 configuration of the experimental setup for compression testing and real-time electronical resistance measurement: (a) and (b) the test fixture for different loading conditions; (c) schematic diagram of the Kelvin Four-terminal sensing method for the smart CCFTCS self-monitoring; (d) KeySight Agilent 34970A data collector and software.

3. Results and discussions

3.1. Mechanical-electrical behaviors of CCFTCSs during lateral compression

Fig. 3 (a) plots the force-displacement curves of the CCFTCSs for the three different layer thicknesses during quasi-static lateral compression which presented similar elastic-plastic nonlinear tendency, demonstrating three deformation stages, namely elastic stage, progressive crushing stage, and internal self-contact stage [34]. At

the elastic stage, the applied force presented an approximately linear increase. After reaching the peak, the formation of cracks at the hinges of the CCFTCSs led to a substantial decrease in the crushing force. Notice that with the decrease in layer thickness, the lateral compression carrying capacity of the CCFTCSs was improved as the density of carbon fiber reinforcement was essentially increased.

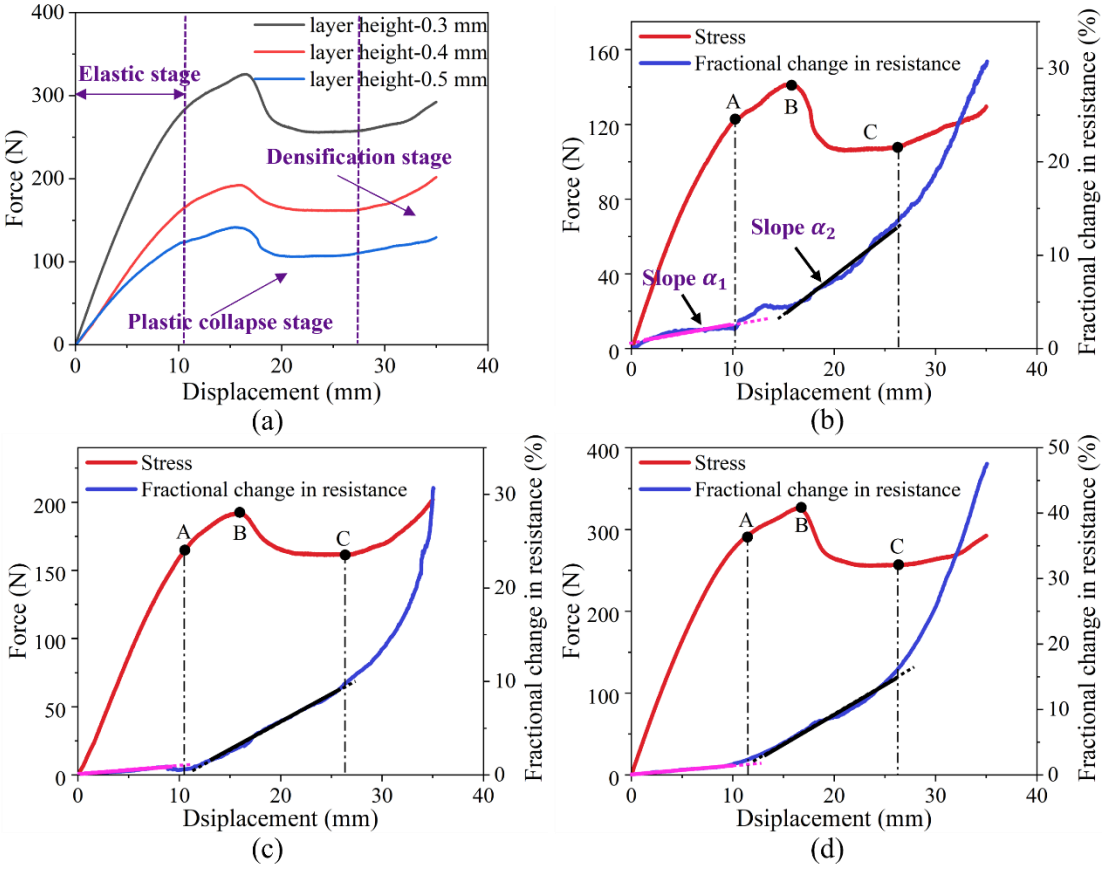

Fig. 3. (a) Compressive force versus displacement curve of CCFTCSs with different layer thicknesses during quasi-static lateral compression, and fractional change in resistance and force versus displacement curves during quasi-static lateral compression with different layer thicknesses: (b) 0.5 mm, (c) 0.4 mm, and (d) 0.3 mm. The elastic point A, ultimate strength point B and plastic collapse point C from the force-displacement curves were marked to describe the relationship between the fractional

change in resistance and compression displacement.

The effect of layer thickness on the evolution of electrical resistance during the quasi-static lateral compression was shown in **Fig**. 3 (b-d). The relative fractional change in resistance was given as:

$$\frac{\Delta R}{R_0} = \frac{R_t - R_0}{R_0}$$

where R_0 represented the initial resistance, R_t represented the resistance at time t.

Three representative points (A, B and C) from the force-displacement curves were selected as reference points for comparing and analyzing the mechanical-electrical behaviors: Elastic point A to check deformation measurement within the elastic stage, plastic collapse point C to detect structure damage in the plastic collapse stage, and point B at the peak of the force-displacement curve to evaluate the ultimate strength of CCFTCSs.

As shown in **Fig**. 3 (b-d), the fractional change in resistance of CCFTCSs with varying layer thicknesses exhibited similar increasing trends as compression displacement increased. Notably, the fractional change in resistance versus displacement curves display two distinct linear relationships at the elastic and progressive crushing stages, respectively. This pattern provides potential avenues for deformation sensing and damage monitoring. **Table** 1 summarizes the slopes (α_1 and α_2) and the correlation coefficients (R^2) of the fitting lines (dash lines in Fig. 3 (b-d)) in both the stages. The high values of the correlation coefficients (R^2) in both elastic

stage and progressive crushing stageindicate an exceptionally linear relationshipbetween the fractional change in resistance and compression displacement. It can be seen that the slopes in the progressive crushing stage were at least 5 times those in the elastic stage. The dramatic change of slope from α_1 to α_2 implies that the progressive crushing stage is reached. This can potentially serve as an indication of the initiation of structural damage that should be circumvented in engineering applications.

Table 1

Slopes (α_1 and α_2) and correlation coefficients (R^2) of the fractional change in resistance versus displacement fitting lines for the CCFTCSs under quasi-static lateral compression.

Layer thickness	Elastic stage		Progressive crushing stage	
	α_1	R^2	α_2	R^2
0.5 mm	0.078	0.946	0.475	0.968
0.4 mm	0.100	0.989	0.602	0.998
0.3 mm	0.152	0.981	0.843	0.991

The fractional change in resistance increased slightly with compression displacement (less than 2.5%) at the elastic stage. The external load in the elastic stage only introduced certain degree of elongation in the continuous carbon fiber, with no fiber damaged occurring, which resulted in a reversible and relatively minor resistance change [35]. **Fig. 4** presents the deformation histories of the CCFTCSs with three different layer thicknesses at the three reference points. After the elastic point A, the

cracks in PLA resin appeared at the vertical (upper or lower) hinges of the CCFTCSs and developed into axial fractional lines as shown in **Fig.** 4 (a2), (b2) and (c2). These cracks did not cause an instantaneous fiber rupture at this stage; instead, it triggered a crack propagation process from the matrix to the fiber [36], resulting in a gradual rupture of the carbon fiber under the load as compression progressed. Consequently, the fractional change in resistance at the progressive crushing stage also showed a linear relationship with displacement, despite the presence of matrix cracks and fiber breaks.. When the applied force reached the ultimate strength point B, minor disturbances of the fractional change in resistance, attributable to abrupt force alterations, were detected. As shown in **Fig.** 4 (a4), (b4) and (c4), the formation of axial fracture lines at all plastic hinges of the CCFTCSs indicate severe damage to the carbon fiber at point C, leading to an exponential increase in the fractional change in resistance.

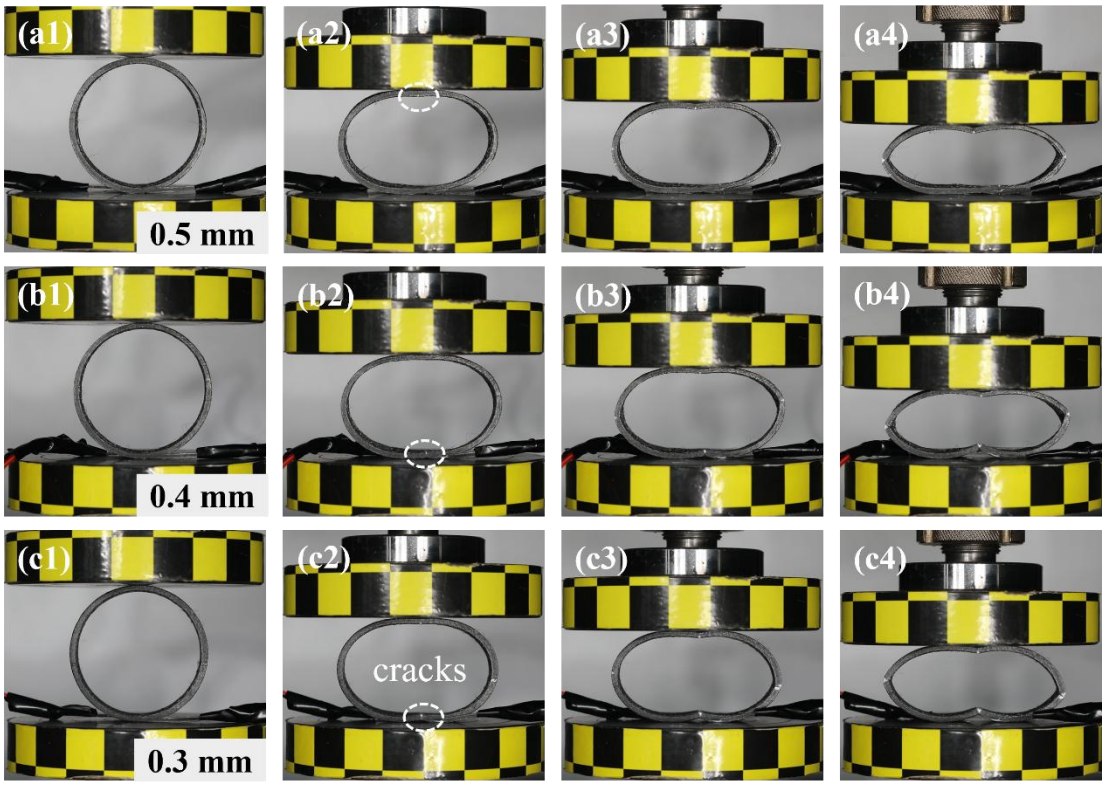

Fig.4. Deformation histories of the CCFTCSs with three different layer thicknesses under quasi-static lateral compression.

An optical microscope was employed to investigate the damage patterns and the failure details of the CCFTCSs at plastic collapse point C as shown in Fig. 5. Here the sample with 0.3 mm layer thickness was chosen as a reference. It was evident that the resin cracks throughout the entire thickness at the bottom of the sample in **Fig.** 5 (c). As observed in the magnified image presented in **Fig.** 5 (d), fractures occurred in a portion of the carbon fiber filament,resulting in an irreversible increase in resistance (Fig. 3(d)). Nevertheless, some carbon fiber filaments remained intact, ensuring the unimpeded transmission of electrical signals. As regards the horizontal hinge, stress-

induced matrix bleaching was observed (**Fig.** 5b), a phenomenon indicative of crack formation. The rupture of carbon fiber at the horizontal hinge leads to the end of the linear relationship and the beginning of the exponential increase in electrical resistance.

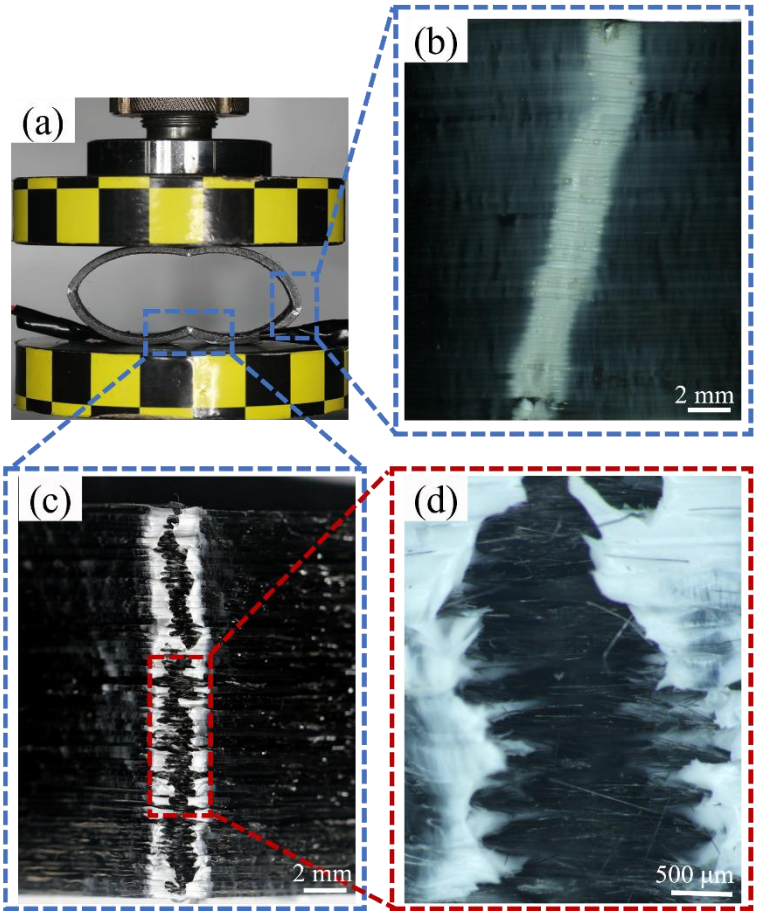

Fig. 5 Micrograph of CCFTCS sample (layer thickness of 0.3 mm) at plastic collapse point C: (a) overall view of the specimen; the distinct axial fractional line of (b) horizontal hinge and (c) vertical hinge; (c) local view of the fractures interface of the vertical hinge.

3.2. Mechanical-electrical behaviors of CCFTCSs during axial compression

Fig. 6 (a) presents the force-displacement curves of the CCFTCSs with three different layer thicknesses under quasi-static axial compression. The compression-

induced crushing behaviors of CCFTCSs can be categorized as progressive stage and catastrophic stage [37]. The crushing curves of CCFTCSs through an initial elastic zone until the first peak was attained, following which the commencement of breaking failure results in a decrease in the load. At catastrophic stage, an increase in load was observed, which can be attributed to the densification of the sample due to section folding. Nonetheless, the decrease in layer height also enhanced significantly the axial compression carrying capacity of the CCFTCSs.

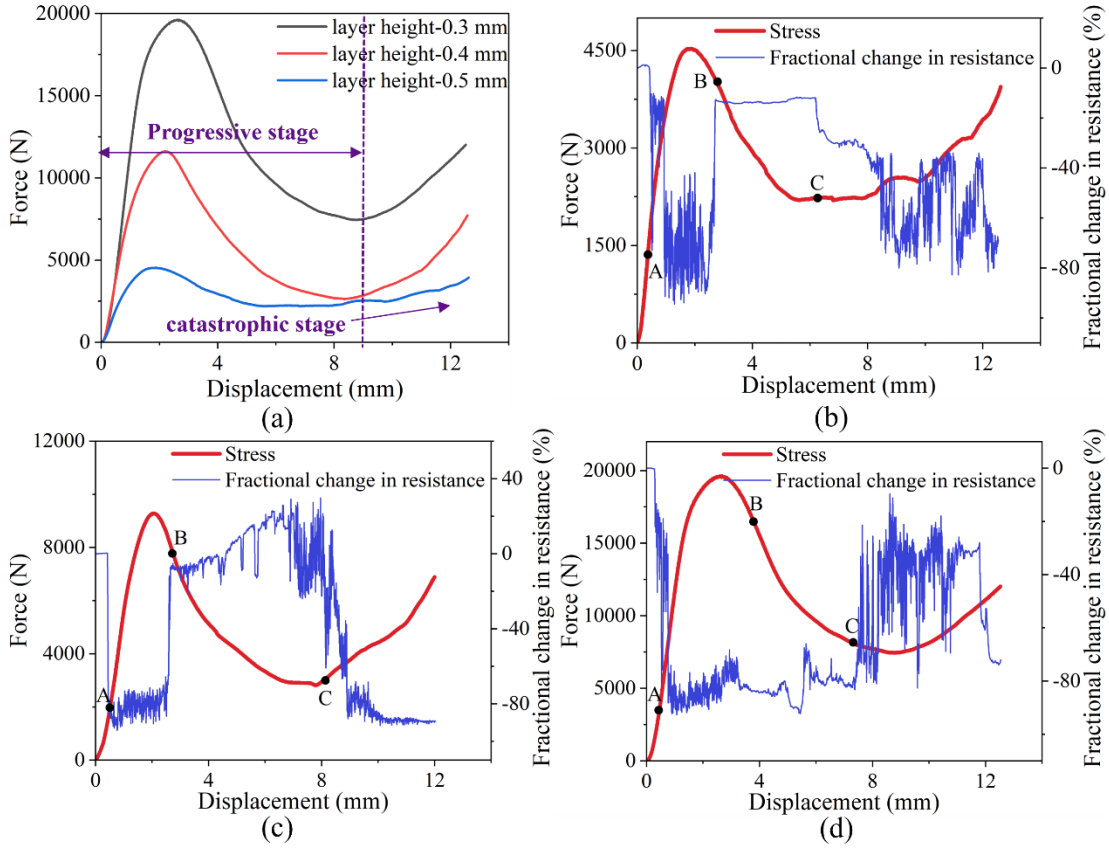

Fig. 6 (a) Compression force versus displacement curves of CCFTCSs with different layer thicknesses under quasi-static axial compression, and fractional changes in resistance and force versus displacement curves under quasi-static axial compression with different layer thickness: (b) 0.5 mm, (c) 0.4 mm, and (c) 0.3 mm. The compaction point A, instability point B and failure point C from the force-displacement curves were

marked to describe the relationship between the fractional change in resistance and compression displacement.

The force and fractional change in resistance versus displacement curves of CCFTCSs during axial compression are shown in **Fig.** 6 (b-d) for different layer thicknesses. Analogously, three representative compression displacement points (Points A, B, C) were chosen from the force-displacement curves to elucidate the correlation between the variations in force and resistance . The three points corresponded to the three reference points of the fractional change in resistance where significant variation occurs. Compaction point A was selected at the linear elastic regime to investigate the reason for the precipitous decline in resistance. Instability point B was chosen as the reference for examining alterations in damage patterns. Failure point C was near the end of the progressive stage to analyze the crushing patterns.

The trends of the fractional change in resistance represented were generally similar for CCFTCSs with different layer thicknesses under axial compression. As demonstrated in **Fig.** 6 (b-d), the fractional change in resistance underwent a rapid decrease at the initial stage of compression. Attributable to the fiber-to-fiber contact induced by in-plane and through-thickness fiber waviness, CFRCs maintained a measurable non-zero conductivity [38]. As illustrated in **Fig.** 7a, the distribution of continuous carbon fiber within the thermoplastic matrix was depicted. It can be seen that the fibers, instead of aligning straight with the printing direction, exhibited a degree of corrugation. As the compression strain increased, the state of the fiber distribution

changed from what is shown in Fig. 7(a) to that depicted in Fig. 7(b). The contact resistance at the interlaminar interface of CCFRC diminished as a consequence of the enhanced degree of fiber-fiber contact (as shown in **Fig.** 7) [39, 40]. Consequently, after loading the CCFTCSs to the compaction point A, the increased fiber-to-fiber contact led to the formation of novel conductive paths, resulting in the decrease of the fractional change in resistance.

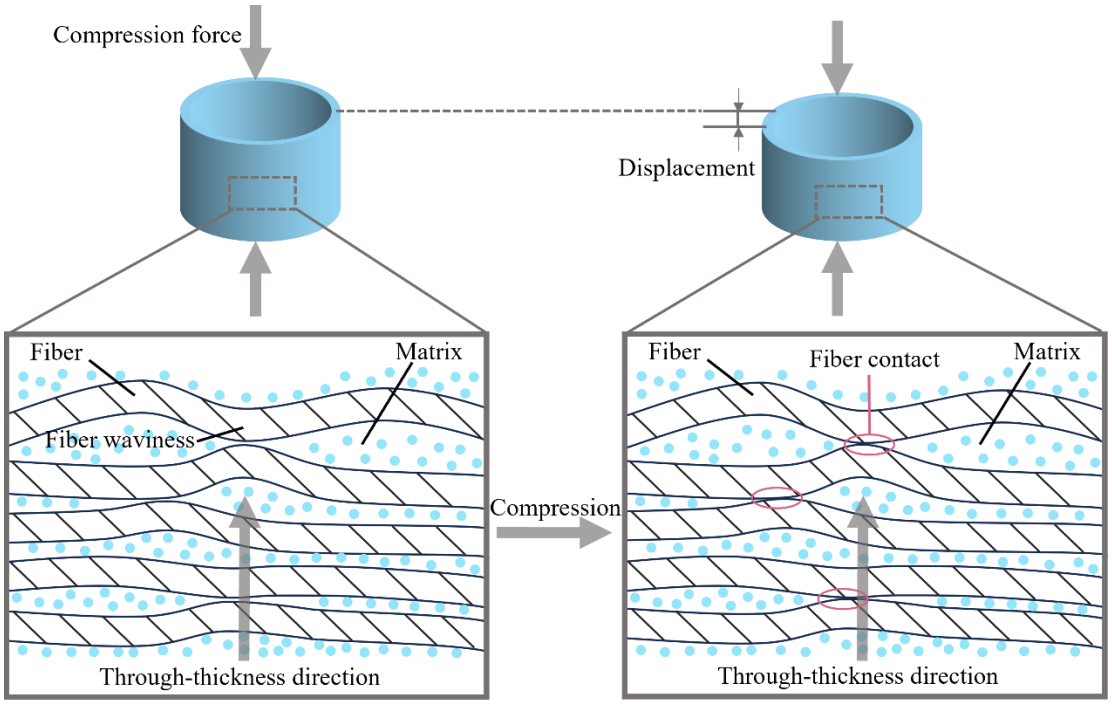

Fig. 7 Schematic illustration of the electrical conduction path associated with through-thickness conduction behavior.

It was evident that the fractional change in resistance exhibited a pattern of descending-ascending-descending throughout the entire loading for CCFTCSs with layer thicknesses of 0.4 mm and 0.5 mm (Fig. 6 (b) and (c)). Meanwhile, the fractional change in resistance in CCFTCSs with a layer thickness of 0.3 mm did not show a

noticeable increase after reaching instability point B; instead, its fluctuations significantly decreased, as shown in Fig. 6(c). **Fig. 8** presents the deformation histories of the CCFTCSs with three different layer thicknesses under axial compression. As the loading reaches the instability point B, As the loading reaches instability point B, the CCFTCSs gradually lose stability and collapse as shown in **Fig.** 8 (a3, b3 and c3). For CCFTCSs with layer thicknesses of 0.5 mm and 0.4 mm, the rising of the fractional change in resistance was attributed to the decrease in fiber-to-fiber contact caused by the depression. For the one with 0.3 mm layer thickness, despite the dispersion of fibers caused by depression, the low layer thickness ensured that the degree of fiber-to-fiber contact remains, resulting in a relatively stable fractional change in resistance. As compression progresses (after the failure point C), the fractional change in resistance for CCFTCSs was observed to exhibit significant fluctuations, indicatingcontinuous alterations in the internal conductive circuit. When the applied force reached the failure point C, some carbon fiber filaments, originally coated by a thermoplastic matrix, were exposed due to cracks in the matrix of the CCFTCSs.. The combined effect of the fracture of carbon fiber (resistance rise) and the formation of new conductive paths through fiber-to-fiber contact (resistance reduction) led to fluctuations in resistance. Therefore, tracking the fluctuating pattern of electrical signal changes is necessary for real-time monitoring of catastrophic damage in CCFTCs.

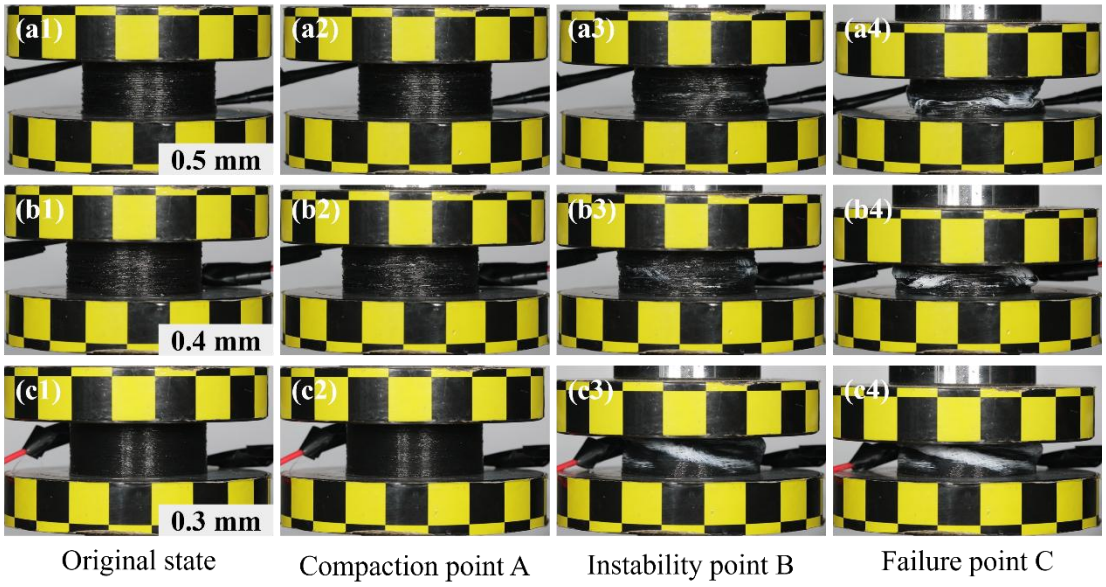

Fig. 8 Deformation histories of the CCFTCSs with three different layer thicknesses under quasi-static axial compression.

To analyze the failure modes of CCFTCSs at a micro level, an optical microscope was presented in **Fig.** 9. Common failure mechanisms of CCFTCSs under quasi-static axial compression included fiber pull-out (**Fig.** 9 (a)), fiber breakage (**Fig.** 9 (b)) and fiber-matrix debonding (**Fig.** 9 (c)). The three modes of failure exerted diverse influences on the resistance. It was obvious that both fiber breakage and fiber-matrix debonding contributed to an increase in resistance. Nevertheless, the fiber pull-out enlarged the free space of carbon fiber and increased the likelihood of the fiber-to-fiber contact, resulting in a complex change in resistance.

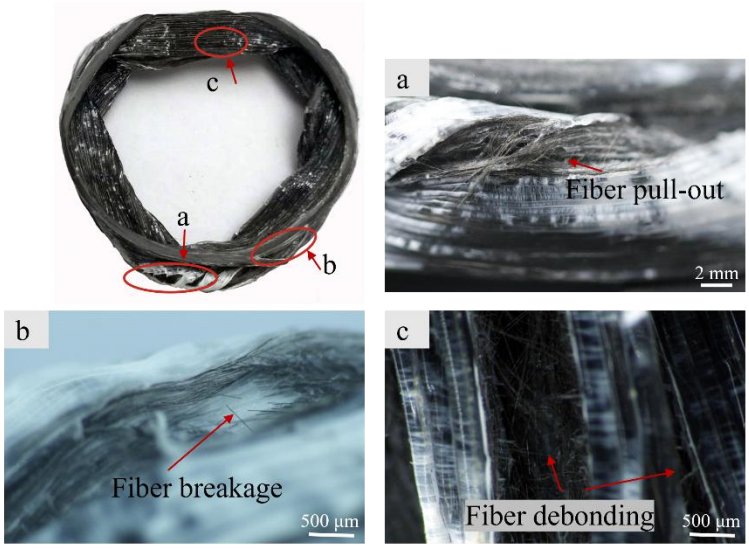

Fig. 9 Micrograph of fractured continuous carbon fiber reinforced thin-walled composite structure specimen.

4. Conclusions

This study investigated the mechanical-electrical behaviors of 3D printed CCFTCSs under quasi-static lateral and axial compression for samples with three different layer thicknesses, i.e., 0.3 mm, 0.4 mm and 0.5 mm. The mechanical-electrical behaviors of continuous carbon fiber offered the potential for electrical-resistance-based self-sensing. The relationship between the external load and the fractional change in resistance at different loading conditions was investigated experimentally with the following conclusions:

Obvious linear relationships between the fractional change in resistance and displacement was observed for the CCFTCSs with three different layer thicknesses under quasi-static lateral compression. Such linear behaviors can be used to determine the deformation stages of CCFTCSs during self-monitoring Under axial compression, due to the through-thickness electrical resistance, the complexity of the fractional

change in resistance of CCFTCSs was amplified. Nevertheless, the catastrophic failures can be still monitored through the electrical resistance measurement. The mechanism of the through-thickness resistance change was also analyzed. A decrease in the fractional change in resistance was observed due to the increased through-thickness fiber contact, which facilitated the formation of new conductive paths. Additionally, complex fiber-matrix failure modes (fiber pull-out, fiber breakage, fiber debonding) caused fluctuations in the fractional change in resistance.

References

[1]A. Baroutaji, M. Sajjia and A.-G. Olabi. On the crashworthiness performance of thin-walled energy absorbers: Recent advances and future developments. Thin-Walled Structures 2017;*118*:137-163.

[2]Q. Liu, H. Shen, Y. H. Wu, Z. C. Xia, J. G. Fang and Q. Li. Crash responses under multiple impacts and residual properties of CFRP and aluminum tubes. Composite Structures 2018;*194*:87-103.

[3]Q. Liu, J. Ma, Z. He, Z. Hu and D. Hui. Energy absorption of bio-inspired multi-cell CFRP and aluminum square tubes. Composites Part B: Engineering 2017;*121*:134-144.

[4]J. Fang, G. Sun, N. Qiu, N. H. Kim and Q. Li. On design optimization for structural crashworthiness and its state of the art. Structural and Multidisciplinary Optimization 2017;*55*(3):1091-1119.

[5]G. Sun, D. Chen, G. Zhu and Q. Li. Lightweight hybrid materials and structures for energy absorption: A state-of-the-art review and outlook. Thin-Walled Structures 2022;*172*:108760.

[6]X. Y. Tian, T. F. Liu, C. C. Yang, Q. R. Wang and D. C. Li. Interface and performance of 3D printed continuous carbon fiber reinforced PLA composites. Composites Part a-Applied Science and Manufacturing 2016;*88*:198-205.

[7]Q. Chen, P. Boisse, C. H. Park, A. Saouab and J. Bréard. Intra/inter-ply shear behaviors of continuous fiber reinforced thermoplastic composites in thermoforming processes. Composite Structures 2011;*93*(7):1692-1703.

[8]P. Mitschang, M. Blinzler and A. Wöginger. Processing technologies for continuous fibre reinforced thermoplastics with novel polymer blends. Composites Science and Technology 2003;*63*(14):2099-2110.

[9]Q. Liu, J. Ma, X. Xu, Y. Wu and Q. Li. Load bearing and failure characteristics of perforated square CFRP tubes under axial crushing. Composite Structures 2017;*160*:23-35.

[10]R. Yang and Y. He. Polymer-matrix composites carbon fibre characterisation and damage inspection using selectively heating thermography (SeHT) through electromagnetic induction. Composite Structures 2016;*140*:590-601.

[11]P. Cheng, Y. Peng, K. Wang, Y.-Q. Wang and C. Chen. Study on intralaminar crack propagation mechanisms in single- and multi-layer 2D woven composite laminate. Mechanics of Advanced Materials and Structures 2022;*29*(25):4310-4318.

[12]P. Cheng, Z. Ye, Y. Huang, D. Wang, Y. Peng, K. Wang and S. Ahzi. Electrical resistance-based self-monitoring of manufacturing damage in 3D printed continuous carbon fiber reinforced composites. Composites Communications 2023;*43*:101749.

[13]P. Kudela, M. Radzieński and W. Ostachowicz. Identification of cracks in thin-walled structures by means of wavenumber filtering. Mechanical Systems and Signal Processing 2015;*50-51*:456-466.

[14]P. Zhuo, S. Li, I. A. Ashcroft and A. I. Jones. Material extrusion additive manufacturing of continuous fibre reinforced polymer matrix composites: A review and outlook. Composites Part B: Engineering 2021;*224*:109143.

[15]O. Gohardani, M. C. Elola and C. Elizetxea. Potential and prospective implementation of carbon nanotubes on next generation aircraft and space vehicles: A review of current and expected applications in aerospace sciences. Progress in Aerospace Sciences 2014;*70*:42-68.

[16]C. C. Luan, X. H. Yao, C. Zhang, J. Z. Fu and Ben W. a. n. g. . Integrated self-monitoring and self-healing continuous carbon fiber reinforced thermoplastic structures using dual-material three-dimensional printing technology. Composites Science and Technology 2020;*188*.

[17]C. Q. Yang, X. L. Wang, Y. J. Jiao, Y. L. Ding, Y. F. Zhang and Z. S. Wu. Linear strain sensing performance of continuous high strength carbon fibre reinforced polymer composites. Composites Part B-Engineering 2016;*102*:86-93.

[18]M. N. Saleh, A. Yudhanto, G. Lubineau and C. Soutis. The effect of z-binding yarns on the electrical properties of 3D woven composites. Composite Structures 2017;*182*:606-616.

[19]W. G. Ye, H. Dou, Y. Y. Cheng, D. H. Zhang and S. Lin. Mechanical and self-sensing properties of 3D printed continuous carbon fiber reinforced composites. Polymer Composites 2022;*43*(10):7428-7437.

[20]C. F. Han, S. W. Huang, B. Z. Sun and B. H. Gu. Electrical resistance changes of 3D carbon fiber/epoxy woven composites under short beam shear loading along different orientations. Composite Structures 2021;*276*.

[21]P.-S. Shin, J.-H. Kim, Y.-M. Baek, H.-S. Park, D.-J. Kwon, S.-O. Moon, K. L. DeVries and J.-M. Park. New evaluation of interfacial and mechanical properties of thermally- treated Pine/CFRP composites using electrical resistance measurement. Composites Part B: Engineering 2018;*151*:139-147.

[22]S. Liu, Y. Luan, Y. Li, Q. Su, Z. Guo and W. Song. A 3D printed continuous carbon fiber reinforced composite with function of self-detecting and self-healing of internal damages. Composites Science and Technology 2023;*243*:110264.

[23]S. Wang and D. D. L. Chung. Self-sensing of flexural strain and damage in carbon fiber polymer-matrix composite by electrical resistance measurement. Carbon 2006;*44*(13):2739-2751.

[24]S. K. Wang, D. D. L. Chung and J. H. Chung. Self-sensing of damage in carbon fiber polymer-matrix composite by measurement of the electrical resistance or potential away from the damaged region. Journal of Materials Science 2005;*40*(24):6463-6472.

[25]F. Mashayekhi, J. Bardon, V. Berthé, H. Perrin, S. Westermann and F. Addiego. Fused Filament Fabrication of Polymers and Continuous Fiber-Reinforced Polymer Composites: Advances in Structure Optimization and Health Monitoring. Polymers 2021;*13*(5):789.

[26]P. Cheng, Y. Peng, S. Li, Y. Rao, A. Le Duigou, K. Wang and S. Ahzi. 3D printed continuous fiber reinforced composite lightweight structures: A review and outlook. Composites Part B: Engineering 2023;*250*:110450.

[27]X. H. Yao, C. C. Luan, D. M. Zhang, L. J. Lan and J. Z. Fu. Evaluation of carbon fiber-embedded 3D printed structures for strengthening and structural-health monitoring. Materials & Design 2017;*114*:424-432.

[28]Q. R. Wang, X. Y. Tian, L. Huang, D. C. Li, A. V. Malakhov and A. N. Polilov. Programmable morphing composites with embedded continuous fibers by 4D printing. Materials & Design 2018;*155*:404-413.

[29]Z. W. Wang, C. C. Luan, G. X. Liao, X. H. Yao and J. Z. Fu. Mechanical and self-monitoring behaviors of 3D printing smart continuous carbon fiber-thermoplastic lattice truss sandwich structure. Composites Part B-Engineering 2019;*176*.

[30]J. Wang, Y. S. Liu, K. Wang, S. Yao, Y. Peng, Y. N. Rao and S. Ahzi. Progressive collapse behaviors and mechanisms of 3D printed thin-walled composite structures under multi-conditional loading. Thin-Walled Structures 2022;*171*.

[31]P. Cheng, K. Wang, X. Z. Chen, J. Wang, Y. Peng, S. Ahzi and C. Chen. Interfacial and mechanical properties of continuous ramie fiber reinforced biocomposites fabricated by in-situ impregnated 3D printing. Industrial Crops and Products 2021;*170*.

[32]A. K. Mishra, H. Chavan and A. Kumar. Effect of material variation on the uniaxial compression behavior of FDM manufactured polymeric TPMS lattice materials. Materials Today: Proceedings 2021;*46*:7752-7759.

[33]S. Wen, S. Wang and D. D. L. Chung. Carbon fiber structural composites as thermistors. Sensors and Actuators A: Physical 1999;*78*(2):180-188.

[34]S. F. Li, X. Guo, Q. Li, D. Ruan and G. Y. Sun. On lateral compression of circular aluminum, CFRP and GFRP tubes. Composite Structures 2020;*232*.

[35]N. Kalashnyk, E. Faulques, J. Schjodt-Thomsen, L. R. Jensen, J. C. M. Rauhe and R. Pyrz. Monitoring self-sensing damage of multiple carbon fiber composites using piezoresistivity. Synthetic Metals 2017;*224*:56-62.

[36]C. de Kergariou, H. Saidani-Scott, A. Perriman, F. Scarpa and A. Le Duigou. The influence of the humidity on the mechanical properties of 3D printed continuous flax fibre reinforced poly(lactic acid) composites. Composites Part A: Applied Science and Manufacturing 2022;*155*:106805.

[37]U. Morales, A. Esnaola, M. Iragi, L. Aretxabaleta and J. Aurrekoetxea. Quasi-static and dynamic crush behaviour of 3D printed thin-walled profiles reinforced with continuous carbon and glass fibres. Composites Part B: Engineering 2021;*217*:108865.

[38]J. Galos, Y. W. Hu, A. R. Ravindran, R. B. Ladani and A. P. Mouritz. Electrical properties of 3D printed continuous carbon fibre composites made using the FDM process. Composites Part a-Applied Science and Manufacturing 2021;*151*.

[39]D. J. Wang and D. D. L. Chung. Through-thickness stress sensing of a carbon fiber polymer-matrix composite by electrical resistance measurement. Smart Materials & Structures 2007;*16*(4):1320-1330.

[40]D. J. Wang and D. D. L. Chung. Through-thickness piezoresistivity in a carbon fiber polymer-matrix structural composite for electrical-resistance-based through-thickness strain sensing. Carbon 2013;*60*:129-138.